MICROSTRUCTURAL CONSTRAINTS ON THE FORMATION HISTORY OF HIBONITE IN REFRACTORY INCLUSIONS. J. Han[1,2], L. Kööp[3,4], L. P. Keller[2], and A. M. Davis[3–5]. [1]Lunar and Planetary Institute, 3600 Bay Area Boulevard, Houston, TX 77058, USA (jangmi.han@nasa.gov), [2]ARES, Code XI3, NASA Johnson Space Center, 2101 NASA Parkway, Houston, TX 77058, USA, [3]Department of the Geophysical Sciences, [4]Chicago Center for Cosmochemistry, [5]Enrico Fermi Institute, University of Chicago, Chicago, IL 60637, USA.

Introduction: Hibonite is a primary refractory phase occurring in many Ca-Al-rich inclusions (CAIs), typically with spinel and perovskite [1]. Previous microstructural studies of hibonite in CAIs revealed the presence of numerous stacking defects along the (001) plane and correlated non-stoichiometry in hibonite [2,3]. These features are interpreted as complex intergrowths of stoichiometric and Ca-deficient hibonites, as shown by experimental studies of reaction-sintered CaO-Al_2O_3 compounds [4]. Here, we extend our transmission electron microscope (TEM) studies to hibonite-bearing CAIs in CM chondrites that have been well characterized isotopically [5–7].

In addition, we have undertaken a series of annealing experiments to explore the effect of minor elements (Mg and Ti) on the microstucure of hibonite [8,9,this study]. The results of these experiments are being applied to hibonite in CAIs in order to better understand its formation conditions.

Samples and Methods: Building on our earlier annealing studies [8,9], a new experiment was prepared by allowing a $2CaO$-Al_2O_3 eutectic melt containing 5 wt% MgO and $CaTiO_3$ to react with a pure alumina crucible at 1,530°C for ~5 days, followed by air quenching. Two TEM sections were extracted from hibonite in the reaction zone of the run product using a FEI Quanta 3D field emission gun SEM/FIB instrument at NASA JSC.

A spinel-hibonite inclusion (SHIB) 1-9-5 and two platy hibonite crystals (PLACs) 2-7-1 and 2-8-2, recovered by freeze-thaw disaggregation and density separation from the Murchison CM2 chondrite, were also studied using TEM. Hibonite in these two CAI types is compositionally and isotopically distinct [5,6]; SHIB 1-9-5 hibonite contains 2.0–3.1 wt% MgO, whereas hibonite in PLACs 2-7-1 and 2-8-2 contains <1 wt% MgO with no resolvable radiogenic ^{26}Mg excess. PLAC 2-7-1 is unusual in that spinel occurs at its margin [6,10]. The TEM sections of hibonite from the three CAIs were prepared using a Tescan LYRA3 SEM/FIB instrument at University of Chicago [10].

The FIB sections were then examined for structural and chemical characteristic by a JEOL 2500SE field emission scanning TEM equipped with a Thermo-Noran thin window energy dispersive X-ray (EDX) spectrometer at NASA JSC.

Results: *Hibonite in the Reaction Zone.* The new annealing experiment produced a reaction zone similar to that observed in our previous experiments [8,9]. Adjacent to the alumina is a hibonite layer, followed by a grossite layer, and finally a zone of krotite and Ti-bearing residual melt (Fig. 1a). While corundum occurs as numerous inclusions in hibonite, no spinel intergrown with or in contact with hibonite is observed. Instead, abundant euhedral spinel crystals occur as inclusions in both grossite and krotite + melt.

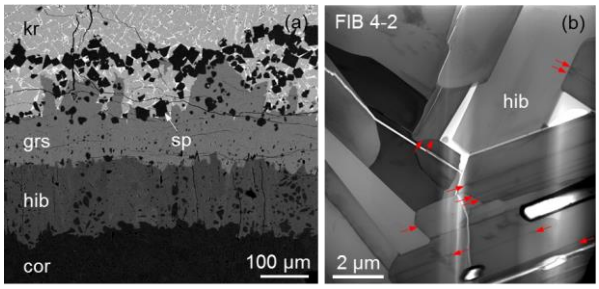

Figure 1. (a) BSE image of the reaction zone from experiment (4) showing a sequence of corundum (cor), hibonite (hib), grossite (grs), and krotite (kr) + melt. (b) BF STEM image of FIB 4-2. Hibonite crystals contain stacking defects indicated by red arrows.

In FIB 4-1 prepared from the middle of the hibonite layer, hibonite is defect-free and pure $CaAl_{12}O_{19}$. Both electron diffraction patterns and lattice fringe images of hibonite show uniform *d*-spacings and 2.2 nm wide (001) spacing. Hibonite in FIB 4-1 represents well ordered, stoichiometric hibonite.

FIB 4-2 cut near the hibonite-grossite interface consists of compact intergrowths of randomly-oriented hibonite laths (Fig. 1b). Hibonite crystals show i) a low density of stacking defects parallel to their elongation direction, ii) weak streaking along the *c* axis in electron diffraction patterns, and iii) random variations in lattice fringe spacing along the *c* axis (e.g., random intergrowths of 2.6 nm (001) spacing within prominent 2.2 nm (001) spacing). Our EDX analyses show that hibonite contains Mg and Ti (<1 wt% MgO and <0.5 wt% TiO_2) and that the stacking defects are clearly linked to an increase in the MgO contents with constant Al_2O_3 and CaO contents. However, defect-rich regions in hibonite appear to be uncorrelated with their TiO_2 content compared to its defect-free regions. Hibonite in FIB 4-2 thus consists of complex, disordered intergrowths of stoichiometric and MgO-enriched hibonites.

Murchison CAIs. Hibonite crystals in both PLACs 2-7-1 and 2-8-2 are free of stacking defects, and show uniform 2.2 nm wide (001) spacing in lattice fringe

images. However, PLAC 2-7-1 contains numerous rounded, strained regions (Fig. 2a) that have slightly distorted, narrower lattice fringes in their center compared to the surrounding hibonite. These structural disturbances accommodate a very minor Al_2O_3 enrichment and correlated CaO and TiO_2 depletions relative to the host hibonite. Additionally, hibonite in PLAC 2-7-1 is partially embayed by intergrowths of spinel and perovskite [10], but has a crystallographic orientation relationship of $(001)_{hib}$ //$(111)_{sp}$ with only spinel.

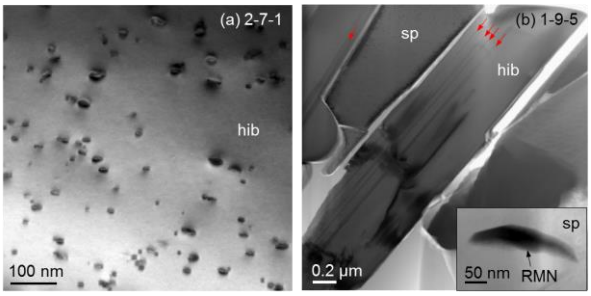

Figure 2. BF STEM images of CAIs 2-7-1 (a) and 1-9-5 (b). In (a), the rounded, strained regions in hibonite are shown in black. In (b), stacking defects in hibonite are indicated by red arrows, and an inset shows a refractory metal nugget (RMN) embedded in spinel.

In contrast, in SHIB 1-9-5, hibonite crystals contain a low density of stacking defects (Fig. 2b). Their microstructural and compositional characteristics are very similar to those observed in FIB 4-2. In addition, spinel is crystallographically oriented to hibonite with $(001)_{hib}$//$(111)_{sp}$. A refractory metal nugget embedded in spinel [10] has a uniform composition of (in wt%) 2 Re, 25 Os, 4 W, 15 Ir, 10 Mo, 17 Ru, 12 Pt, 3 Rh, 2 Ni, and 10 Fe. These elements show approximately a flat pattern with enrichment factors of ~1–5×10^5 on a CI-normalized diagram.

Discussion: Our new experiment produced hibonite that contains a range of stacking defect densities and correlated compositional variations, consistent with the results of our previous experiments [8,9]. The similar characteristics are also observed in hibonite from the Murchison CAIs. These characteristics of hibonite can be explained by the arrangement of two basic spinel and Ca-containing blocks [3,4] and the preferential substitution of Mg and Ti in hibonite [11]. The MgO enrichments along stacking defects in hibonite are therefore direct evidence that the substitution of Mg with Al in the spinel blocks stabilized the formation of wider spinel blocks in hibonite, hence forming complex intergrowths of stoichiometric and disordered, Mg-enriched hibonite [3]. The lack of a correlation between the presence of stacking defects and the TiO_2 contents may suggest that the substitution of Ti with Al in the Ca-containing blocks is not an important mechanism to form stacking disorder (e.g., wider Ca-containing blocks) in hibonite. However, a much lower density of stacking defects in Mg,Ti-bearing hibonite in our new experiment compared to only Mg-bearing hibonite in our previous experiments [8,9] suggests that the introduction of Ti during the formation of hibonite appears to have inhibited the substitution of Mg with Al in the spinel blocks. An additional TEM study of synthetic and meteoritic hibonites is underway to investigate in more detail the effect of Ti on the formation of stacking disorder in hibonite.

Hibonite in PLACs 2-8-2 and 2-7-1 appears to have condensed stoichiometrically before ^{26}Al arrival in the solar nebula [6]. The strained regions in PLAC 2-7-1 hibonite may represent regions where $Al_{8/3}O_4$-rich spinel nucleated metastably at the very early stages of the formation of wider spinel blocks (i.e., stacking defects) in hibonite. Later, spinel nucleated epitaxially and grew onto hibonite by reaction of hibonite and gaseous Mg, as indicated by their crystallographic orientation relationship, during condensation of perovskite.

The lack of the original textural context of SHIB 1-9-5 makes it difficult to infer its origin. Thus, defect-structured hibonite in this inclusion may have formed metastably by direct condensation or by melting of an early-condensed refractory assemblage as Mg was incorporated into hibonite as extra spinel blocks (i.e., stacking defects). Spinel nucleated and grew in a crystallographic continuity with hibonite and then coninuted to form into larger crystals.

Conclusions: Our TEM study shows a microstructural difference between Muchison PLAC and SHIB hibonites, consistent with their different formation conditions, as inferred by their isotope compositions [5,6]. Combined with the results of our annealing experiments [8,9,this study], this difference can be interpreted as the result of the accommodation of non-stoichiometry in hibonite by altering stacking sequence of spinel and Ca-containing blocks in the ideal hibonite structure [3,4].

Acknowledgements: This study was supported by NASA grants EW14-2-122 to LPK and NNX15AF76G to AMD.

References: [1] MacPherson G. J. (2014) Treatise on Geochemistry II vol.1 pp.139-179. [2] Keller L. P. (1991) AGU 72, 141. [3] Han J. et al. (2015) MAPS 50, 2121-2136. [4] Schmid H. & De Jonghe L. C. (1983) Philos. Mag. A 48, 287-297. [5] Kööp L. et al. (2016) GCA 184, 151-172. [6] Kööp L. et al. (2016) GCA 189, 70-95. [7] Liu M.-C. et al. (2012) EPSL 327-328, 75-83. [8] Han J. et al. (2016) 47th LPSC #2848. [9] Han J. et al. (2016) 79th MetSoc #6534. [10] Kööp L. et al. (2016) 47th LPSC #2005. [11] Doyle P. M. et al. (2014) AM 99, 1369-1382.